Investigation of the Photochemical Reactivity of Soot Particles Derived from Biofuels Toward NO 2 . A Kinetic and Product Study

ARTICLE *in* THE JOURNAL OF PHYSICAL CHEMISTRY A · FEBRUARY 2015

Impact Factor: 2.69 · DOI: 10.1021/jp511468t · Source: PubMed

THE JOURNAL OF PHYSICAL CHEMISTRY A

Article

pubs.acs.org/JPCA

Investigation of the Photochemical Reactivity of Soot Particles Derived from Biofuels Toward NO_2. A Kinetic and Product Study

Manolis N. Romanías,*[,†] Philippe Dagaut,*[,†] Yuri Bedjanian,[†] Auréa Andrade-Eiroa,[†] Roya Shahla,[†] Karafas S. Emmanouil,[‡] Vassileios C. Papadimitriou,[§] and Apostolos Spyros[‡]

[†]Institute de Combustion, Aérothermique, Réactivité et Environnement (ICARE)-CNRS, 1C Avenue de la Recherche Scientifique, 45071, Orléans, France

[‡]NMR Laboratory, Department of Chemistry, University of Crete, Vassilika Vouton, 71003, Heraklion, Crete, Greece

[§]Laboratory of Photochemistry and Chemical Kinetics, Department of Chemistry, University of Crete, Vassilika Vouton, 71003, Heraklion, Crete, Greece

Supporting Information

ABSTRACT: In the current study, the heterogeneous reaction of NO_2 with soot and biosoot surfaces was investigated in the dark and under illumination relevant to atmospheric conditions (J_{NO_2} = 0.012 s^{-1}). A flat-flame burner was used for preparation and collection of soot samples from premixed flames of liquid fuels. The biofuels were prepared by mixing 20% v/v of (i) 1-butanol ($CH_3(CH_2)_3OH$), (ii) methyl octanoate ($CH_3(CH_2)_6COOCH_3$), (iii) anhydrous diethyl carbonate $(C_2H_5O)_2CO$ and (iv) 2,5 dimethyl furan $(CH_3)_2C_4H_2O$ additive compounds in conventional kerosene fuel (JetA-1). Experiments were performed at 293 K using a low-pressure flow tube reactor (P = 9 Torr) coupled to a quadrupole mass spectrometer. The initial and steady-state uptake coefficients, γ_0 and γ_{ss}, respectively, as well as the surface coverage, N_s, were measured under dry and humid conditions. Furthermore, the branching ratios of the gas-phase products NO (~80−100%) and HONO (<20%) were determined. Soot from JetA-1/2,5-dimethyl furan was the most reactive [$\gamma_0 = (29.1 \pm 5.8) \times 10^{-6}$, γ_{ss}(dry) = $(9.09 \pm 1.82) \times 10^{-7}$ and γ_{ss}(5.5%RH) = $(14.0 \pm 2.8)^{-7}$] while soot from JetA-1/1-butanol [$\gamma_0 = (2.72 \pm 0.544) \times 10^{-6}$, γ_{ss}(dry) = $(4.57 \pm 0.914) \times 10^{-7}$, and γ_{ss}(5.5%RH) = $(3.64 \pm 0.728) \times 10^{-7}$] and JetA-1/diethyl carbonate [$\gamma_0 = (2.99 \pm 0.598) \times 10^{-6}$, γ_{ss}(dry) = $(3.99 \pm 0.798) \times 10^{-7}$, and γ_{ss}(5.5%RH) = $(4.80 \pm 0.960) \times 10^{-7}$] were less reactive. To correlate the chemical reactivity with the physicochemical properties of the soot samples, their chemical composition was analyzed employing Raman spectroscopy, NMR, and high-performance liquid chromatography. In addition, the Brunauer−Emmett−Teller adsorption isotherms and the particle size distributions were determined employing a Quantachrome Nova 2200e gas sorption analyzer. The analysis of the results showed that factors such as (i) soot mass collection rate, (ii) porosity of the particles formed, (iii) aromatic fraction, and (iv) pre-existence of nitro-containing species in soot samples (formed during the combustion process) can be used as indicators of soot reactivity with NO_2.

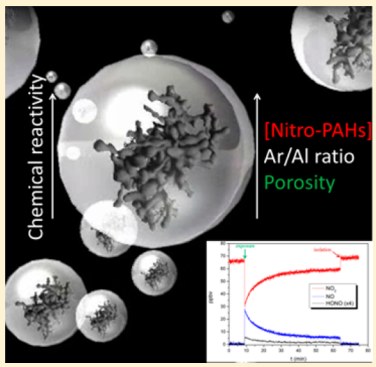

1. INTRODUCTION

One of the major challenges that the human race has been facing over the past decades is the management of energy issues and its impact on environment degradation. The systematic increase of CO_2 and the reduction of fossil fuel resources in combination with increased energy demand, which is projected to grow by 36% until 2030,[1] have led to the urgent need for renewable and sustainable energy sources. Fuels of biological origin, biofuels, could contribute to solving the worldwide energy crisis. Biofuels are generally classified in three generations according to the applied processing technology.[2] The derivatives from vegetable oil and animal fats have been proposed as alternative fuels for diesel. Thorough research studies have shown that biofuels significantly reduce volatile organic compounds (VOCs), CO_2, CO, SO_x, and particulate matter emissions,[3,4] compared to conventional diesel fuel.

Soot (also known as black carbon/brown carbon, BC/BrC) consists of elementary carbon and numerous organic compounds[5−7] and is one of the products of the incomplete combustion of fuels. Soot undergoes regional and intercontinental transport before being removed via precipitation. Thus, it can be found in remote regions of the atmosphere with lower concentrations than in source regions.[8] Soot atmospheric lifetime is estimated to be ~1 week.[9] The major direct impact of the BC/BrC particles on the environment and climate is the scattering and absorption of sunlight. Indirectly, they participate to the formation of clouds acting as condensation nuclei (CCN). Both processes can significantly influence the radiation balance of the planet. In addition, because of its

Received: November 16, 2014
Revised: February 14, 2015

DOI: 10.1021/jp511468t
J. Phys. Chem. A XXXX, XXX, XXX−XXX

porous nature providing large surface areas, soot can participate in heterogeneous reactions with gas-phase compounds, influencing the chemical composition of the troposphere.[10]

The chemical reactivity of soot has been studied extensively in the past using conventional fuels or fuel-imitative compounds (see refs 11−13 and references therein). In some cases, e.g., NO_2 uptake on soot, significant discrepancies between the literature data were observed (~2 orders of magnitude for uptake coefficients). However, the reactivity of soot produced in combustion of biofuels under relevant atmospheric conditions has not yet been investigated. Because biofuels are already commercially available, and others are projected to be released to the market, it is important to investigate the impact of biosoot on the environment.

To this end, we investigated the chemical reactivity of biosoot samples. NO_2 was used as reference pollutant molecule of the NO_x family because it is known to participate in several heterogeneous reactions producing HONO and acting as regulating agent for O_3 formation. Specifically, the uptake coefficient, γ, and the surface coverage of NO_2, N_s, were measured, and the branching ratio of the gas-phase products was defined using a low-pressure flow tube reactor coupled to a mass spectrometer. Furthermore, the physicochemical properties and chemical composition of soot derived from conventional kerosene and biokerosene fuels were also investigated. The ultimate goal of this work was to correlate the reactivity of soot with its chemical composition. To this end, solid soot samples have been analyzed with Raman and nuclear magnetic resonance (NMR) spectroscopy and with high-performance liquid chromatography (HPLC). Furthermore, the Brunauer−Emmett−Teller (BET) surface areas and particle size distributions were determined using a Quantachrome gas sorption analyzer. To the best of our knowledge, this is the first experimental study in which the reactivity and the physicochemical properties of soot and biosoot particles have been investigated together.

2. EXPERIMENTAL SECTION

2.1. Biofuels Preparation: Chemicals. All the chemicals used in the current study were commercially available with stated purity or synthesized. Kerosene (JetA-1) was used as conventional fuel. The biofuels were prepared by diluting 20% v/v of each additive compound with kerosene. The additives used were (i) 1-butanol ($CH_3(CH_2)_3OH$), JetA-1/1-BNOL; (ii) methyl octanoate ($CH_3(CH_2)_6COOCH_3$), JetA-1/MOC; and (iii) anhydrous diethyl carbonate $(C_2H_5O)_2CO$, JetA-1/DEC and (iv) 2,5 dimethyl furan $(CH_3)_2C_4H_2O$, JetA-1/2,5-DMF supplied by Sigma-Aldrich with stated purity ≥99%. In the remainder of the paper, for brevity, the biofuels will be referred to by only their abbreviated names given above. NO_2 was supplied from Air Liquide and was further diluted in He to prepare 5.19% NO_2/He mixture in a 10 L glass bulb. Furthermore, NO and HONO were also used because they comprise the major gas-phase products of the heterogeneous reaction and their concentrations need to be measured to determine the yields of their formation. NO was premixed with He (29.41% NO/He) inside a 6 L glass bulb, while HONO was generated in situ via the following heterogeneous reaction of HCl with $NaNO_2$:

$$HCl + NaNO_2 \rightarrow HONO + NaCl \quad (1)$$

HCl (5% in He, Air Liquide) was flowed through a column containing $NaNO_2$ crystals (purity ≥99%, Sigma-Aldrich), and the heterogeneously formed HONO was injected through the reactor side arm and detected at its parent peak $HONO^+$ (m/z = 47). The concentrations of NO_2 and NO were determined by separate calibration experiments in which the pressure drop at the high-pressure end of a known volume of the gas introduction line was recorded as a function of time. Regarding HONO, absolute concentrations were determined by chemically converting it to NO_2 via the fast reaction with F atoms (produced from microwave discharge of 5% F_2 in He, Air Liquide) that was quantitatively measured:

$$F + HONO \rightarrow HF + NO_2 \quad (2)$$

2.2. Preparation of Soot Surfaces. A flat-flame burner was used for the combustion of kerosene and biokerosene fuels under well-characterized and controlled conditions (Table S1 of the Supporting Information). A simplified scheme and a detailed description of the soot production and collection system has been presented elsewhere and is also given in Figure S1 of the Supporting Information.[13,14] Soot samples were prepared under fuel-rich conditions, $2.2 < \Phi < 2.3$, and deposited onto the outer surface of a Pyrex rod tube at a height 4 cm above the head of the burner. The tube was introduced perpendicular to the flame axis, rotated, and moved through the flame. The sampling Pyrex rod was thermostated at 45 °C by circulating water to avoid temperature gradients which affect the distribution homogeneity of light deposited compounds along the tube during the sampling process.[15,16] The deposited mass of the soot was measured with a highly accurate mass balance upon mechanical removal from the glass tube. The soot collection rate (in milligrams per minute) for each fuel studied is presented in Figure 1. Using conventional kerosene as reference fuel (collection rate, 0.50 mg min^{-1}), it was observed that soot mass collection rate of JetA-1/1-BNOL and JetA-1/DEC biofuels were significantly decreased, 0.17 mg min^{-1} and 0.25 mg min^{-1} respectively, while that for JetA-1/MOC was similar to that JetA-1 (0.55 mg min^{-1}). On the contrary, for JetA-1/2,5-DMF biofuel the measured collection rate was

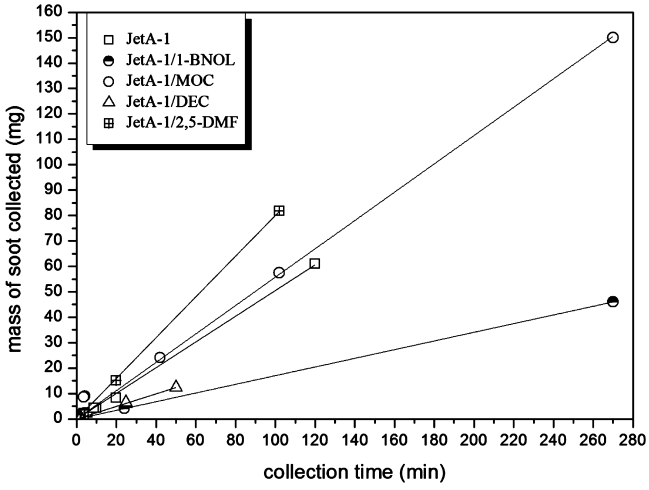

Figure 1. Total mass of soot deposited versus collection time. The soot collection rate was (a) 0.50 mg min^{-1} for pure kerosene, JetA-1 (squares); (b) 0.17 mg min^{-1} for JetA-1/1-BNOL (half filled circles); (c) 0.25 mg min^{-1} for JetA-1/DEC (triangles); (d) 0.55 mg min^{-1} for JetA-1/MOC (open circles); and (e) 0.80 mg min^{-1} for JetA-1/2,5-DMF (cross-filled squares). Solid lines are the linear fits to the experimental data.

DOI: 10.1021/jp511468t
J. Phys. Chem. A XXXX, XXX, XXX−XXX

increased (0.80 mg min^{-1}). Furthermore, thermochemical calculations using the Chemkin suite[17] showed that the flames had different adiabatic temperatures (Table S1 of the Supporting Information), but they were within 10% of that of the reference JetA-1. Nevertheless, as presented in Table S1, no correlation between the temperature of each flame and the sooting mass trends mentioned above was observed.

2.3. BET Surface Area Measurements and Pore Size Distribution. Nitrogen adsorption measurements were performed with a Quantachrome Nova 2200e gas sorption analyzer. The specific surface area of the collected soot samples was determined employing the BET method within 0.05−0.3 relative pressures, P/P_0. Furthermore, non-local density function theory (NLDFT) was used to simulate the adsorption−desorption isotherms and the pore size distribution of the particles was determined. DFT methods have found numerous applications for calculating pore size distribution of micro- and mesoporous solid materials, especially on carbon surfaces.[18−22] DFT provides a microscopic treatment of sorption phenomena at the molecular level based on statistical mechanisms. Its validity has been tested against experimental adsorption isotherms of mesoporous crystal solids with well-characterized cylindrical pores.[23,24]

2.4. Chemical Reactivity Measurements. The chemical degradation of NO_2 on soot surfaces was studied using a low-pressure flow tube reactor (FT), which is shown in Figure S1 of the Supporting Information. Helium was used as carrier gas. The reactor was coupled to a modulated molecular beam quadrupole mass spectrometer (QMS) for the detection of gas-phase species. The FT/QMS technique has been used in the past to study the heterogeneous interaction between gas and bulk aerosol surfaces.[25−28] Thus, only a brief description of the experimental setup is presented here. The experimental setup consists of 3 parts: (i) the gas storage/supply vacuum line, (ii) the flow tube reactor (2.4 cm i.d.), and (iii) the differentially pumped stainless steel high-vacuum chamber that hosts the quadrupole mass spectrometer (Balzers, QMG 420). Externally, the reactor was surrounded by 6 ultraviolet (UV) lamps (Sylvania BL350, 8 W) with a broad UV emission spectrum (315−400 nm). The UV lamps were installed into an aluminum box covering the main reactor tube. The irradiance intensity in the reactor was characterized by direct measurements of the NO_2 photolysis frequency, J_{NO_2}, as a function of the number of lamps switched on.[29] The obtained J_{NO_2} values for 1 and 6 lamps were 0.002 and 0.012 s^{-1}, respectively, corresponding to real photolysis frequencies measured in the atmosphere under cloudy and clear sky conditions.[30−32]

The characteristic parameters that determine the strength of the interaction between a solid surface and a gas molecule are the uptake coefficient, γ, and the surface coverage, N_s. The uptake coefficient can be measured at the initial stage of the surface exposure, γ_0, or at later time, after the surface treatment with the gas molecules has led to a steady state, γ_{ss}. For atmospheric implications, the determination of γ_{ss} is more relevant because soot particles are processed for long periods of time before their final removal and deposition. However, the concept of γ_0 is also important because it is measured on fresh samples, expressing the chemical affinity of a virgin solid surface to a gas pollutant.

In our experimental setup, the uptake coefficient is given by the following expression:

$$\gamma = \frac{4k_{kin}}{\omega} \times \frac{V}{S} \quad \text{(I)}$$

where k_{kin} is the first-order rate coefficient of NO_2 loss (s^{-1}) in the "kinetic regime" (see below), ω the average molecular speed (cm s^{-1}), V the volume of the reaction zone (cm^3), and S the surface area of the deposited sample participating in the reaction (cm^2). Under certain experimental conditions, both ω and V are known parameters of the system; therefore, only k_{kin} and S need to be determined experimentally. Under kinetic regime conditions, when the uptake of the gas molecules is not limited by their diffusion from volume toward the reactive surface, no diffusion corrections are required for determining the k_{kin}. However, when an effective heterogeneous loss leads to an important local depletion of the gas molecules close to the surface, their diffusion from the volume of the reactor toward the surface becomes rate-limiting, which leads to an underestimation of k_{kin} and should be accounted for in the treatment of the experimental data.[25] The diffusion corrections are usually calculated within an approach based on the kinetic resistance additivity rule.[33] In the present study, the applied corrections for the initial uptake were <10%, while those for the steady-state uptake coefficient were <2%.

The total number of molecules accumulated per surface unit, N_s (molecules per square centimeter), can be derived by integrating the area of the adsorption peak in a typical uptake experiment (see also Figure 2) divided by the total soot surface area, S_{BET}, according to the following equation:

$$N_s = \int_{\tau'=0}^{\tau'=t} \frac{F(t')}{S_{BET}}\, dt' \quad \text{(II)}$$

where F is the flow rate (molecule s^{-1}) of NO_2 molecules inside the reactor.

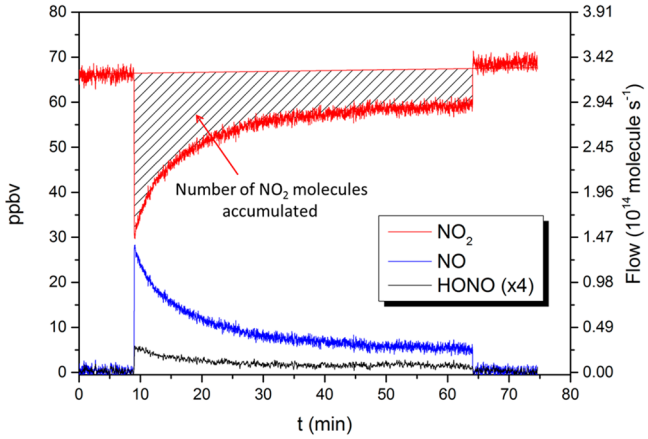

Figure 2. Time-dependent concentration profile of NO_2 (red line) upon reaction with JetA-1/MOC biosoot surface under dark conditions. The production rates of NO (blue line) and HONO (black line) are also presented. The concentration of HONO was multiplied (×4) for presentation purposes.

2.5. Raman Spectroscopy. Spectrometric Raman analyses of soot samples were performed using a Nicolet Almega XP Dispersive Raman spectrometer at λ= 780 nm. The focused area was 10 μm^2, the spectra resolution R = 2 cm^{-1}, and the number of scans was 20.

2.6. Liquid-State NMR Spectroscopy. A small quantity (6.6 mg) of conventional and biokerosene soot samples was

DOI: 10.1021/jp511468t
J. Phys. Chem. A XXXX, XXX, XXX−XXX

Table 1. Summarized Results under Dark Conditions[a]

soot sample	γ_{int} (10^{-6})	γ_{ss} (10^{-7}) dry	γ_{ss} (10^{-7}) 5.5% RH	N_s (10^{13} molecules cm^{-2})[b] dry	N_s (10^{13} molecules cm^{-2})[b] 5.5% RH	S_{BET} (m^2 g^{-1})	Raman $I(D)/I(G)$[c]
JetA-1	5.38 ± 1.01	8.80 ± 1.76	6.12 ± 1.22	5.24 ± 1.04	4.28 ± 0.856	106 ± 10.0	1.41
JetA-1/1-BNOL	2.72 ± 0.544	4.57 ± 0.914	3.64 ± 0.728	3.07 ± 0.610	2.55 ± 0.510	106 ± 10.0	1.23
JetA-1/DEC	2.99 ± 0.598	3.99 ± 0.798	4.80 ± 0.960	2.87 ± 0.570	2.60 ± 0.520	98.0 ± 10.0	1.11
JetA-1/MOC	10.7 ± 2.14	7.92 ± 1.58	9.46 ± 1.89	5.43 ± 1.08	6.27 ± 1.25	110 ± 11.0	1.28
JetA-1/2,5-DMF	29.1 ± 5.82	9.09 ± 1.82	14.0 ± 2.80	8.17 ± 1.63	7.73 ± 1.55	122 ± 12.0	1.45

[a]$[NO_2]$ = 66 ppbv; T = 293 K. [b]Measured after 45 min of exposition. [c]Heavy aromatic/aliphatic fraction of soot.

dissolved in 0.8 mL of $CDCl_3$ and extracted for 1 h in an ultrasonic bath. The solutions were then transferred into a 5 mm NMR tube, and NMR spectra were recorded using a Bruker AVANCE III 500 spectrometer. It should be noted that $CDCl_3$ is a nonpolar solvent; thus, NMR analysis is based on the apolar fraction of soot which has been dissolved. In addition, because of the extraction process performed, the degradation of some aromatic compounds, i.e., polycyclic aromatic hydrocarbons (PAHs), should not be excluded.[34]

2.7. HPLC Analysis. Chromatographic experiments were performed employing a HPLC system from Shimadzu. The instrument consisted of a system controller CBM-20A/20 Alite Prominence, a solvent delivery module LC-20AB Prominence, an autosampler SIL-20A/20AC Prominence, a column oven CTO-20A/20AC Prominence, and an UV−visible photodiode array detector SPD-M20A Prominence. A Vydac column 201TPC18, 5 μm, 250 mm length × 4.6 mm ID (Grace Davison Discovery Sciences), was used for the analysis. Acetonitrile and water were used as mobile phase, and the flow rate was set at 0.5 or 1 mL min^{-1} (depending on the solvent where the fraction is injected). Note that in the general framework of biofuels investigation and their impact on the environment a novel analytical methodology for the detailed chemical characterization of soot samples has been developed in our laboratory.[34] The major advantage of the method developed was the separation of different PAH families of compounds. Details regarding the extraction, clean up, and fractioning protocols have been described previously.[34]

3. RESULTS AND DISCUSSION

3.1. BET Surface Area Measurements and Soot Pore Size Distribution. The BET surface areas of the studied soot samples are given in Table 1. Although there are not dramatic differences between the measured BET, a clear trend has been observed, according to the following order: $S_{BET,\ JetA\text{-}1/2,5\text{-}DMF} > S_{BET,\ JetA\text{-}1/MOC} > S_{BET,\ JetA\text{-}1} = S_{BET,\ JetA\text{-}1/1\text{-}BNOL} > S_{BET,\ JetA\text{-}1/DEC}$. Furthermore, NLDFT was used to simulate the experimental determined N_2 isotherms to extract the pore size distributions of conventional and biosoot samples (Figure S2 of the Supporting Information). The soot particles collected were found to be in the mesoporous scale, in accordance with previous studies.[19,22] To summarize, the results indicate that the additive compounds used to dope kerosene fuel can influence the physical properties of the corresponding BC/BrC particles collected.

3.2. Chemical Reactivity of Soot. The interaction of NO_2 with soot surfaces produced from the combustion of kerosene/biokerosene fuels was studied at T = 293 K and P = 9 Torr. The experiments were performed under dry (0.0032% RH) and humid (5.5% RH) conditions to investigate the role of H_2O in the reaction system. In addition, because BC/BrC particles contain UV-absorbing species, a series of experiments were conducted irradiating soot samples with UV light (J_{NO_2} = 0.012 s^{-1}), probing a potential impact to the reaction system. The results are summarized in Figures 2−7 and in Table 1. A typical time-dependent uptake profile of NO_2 and the corresponding production concentration profiles of NO and HONO (gas-phase products detected) under dark conditions are presented in Figure 2. The initial fast consumption of NO_2 is followed by a rapid recovery to the pre-exposure concentration levels due to the processing of the soot particles and the depletion of the active surface sites. Regarding the reaction products, NO and HONO, one can note that their production rates correlate with the rate of NO_2 loss.

3.2.1. Dependence of the Uptake Coefficient on Soot Thickness. A series of experiments were conducted in which the uptake coefficient was measured as a function of the thickness of soot samples exposed to NO_2. The objective of those experiments was to determine the surface area of the solid film involved in the interaction. Experiments were performed by exposing pure kerosene soot to NO_2 = 66 ppbv at T = 293 K under 5.5% of RH. The results are presented in Figure 3, in which the geometric uptake coefficient is plotted as a function of the soot mass deposited per unity length of the support tube (milligrams per centimeter). The linear dependence of the uptake coefficient on soot mass suggests that the entire surface area of the solid sample is accessible to NO_2; therefore, the BET surface area should be applied for the

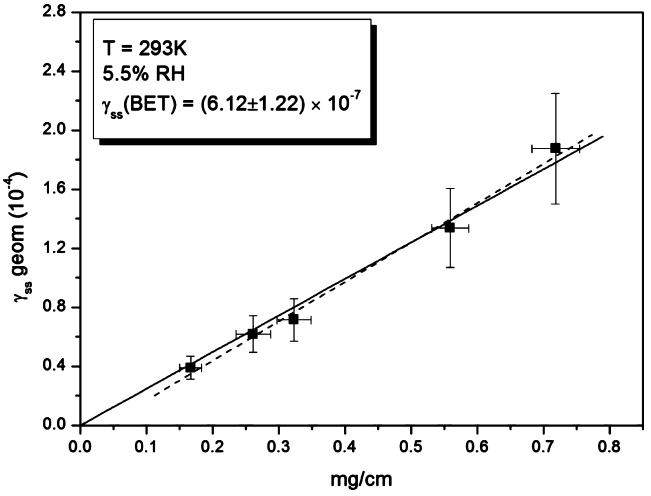

Figure 3. Steady-state uptake coefficient of NO_2 (calculated using geometric surface area) as a function of soot sample mass (per 1 cm length of the support tube): T = 293 K; RH 5.5%; P = 9 Torr; 66 ppbv NO_2; sample mass, 0.16−0.72 mg cm^{-1}. The solid line represents the forced-to-zero least-squares fit, and the dashed line represents the unrestricted least-squares fit.

DOI: 10.1021/jp511468t
J. Phys. Chem. A XXXX, XXX, XXX−XXX

determination of the true steady-state uptake coefficient which is given by the following expression:

$$\gamma_{ss}(\mathrm{BET}) = [\mathrm{slope}\ (\mathrm{cm\ mg^{-1}})]\frac{C\ (\mathrm{cm})}{S_{\mathrm{BET}}\ (\mathrm{cm^2\ mg^{-1}})} \qquad \text{(III)}$$

where the slope is extracted from Figure 3; C is the circumference of the supported glass tube covered with soot, and S_{BET} is the total surface area of soot. Applying the slope of the forced-through-zero linear fit to the experimental data of Figure 3 in eq III gives the steady-state uptake coefficient of NO_2 under the current experimental conditions (T, RH, and $[NO_2]$) as $\gamma_{ssBET} = (6.12 \pm 1.22) \times 10^{-7}$. The given uncertainty reflects the precision of the fit (2σ) and the uncertainty on BET surface area and on the measurements of k_{NO_2}. The least-squares fit to the data was also taken without zero-forcing restrictions (dashed line in Figure 3), and the obtained value of the uptake coefficient is in excellent agreement (within 5%) with that obtained from the forced-through-zero fit.

3.2.2. Uptake Coefficients: Surface Coverage Measurements for Different Soot Samples. The initial uptake coefficient, γ_0, was found to be independent of RH and UV light irradiation conditions (Figure 4). In contrast, it was found

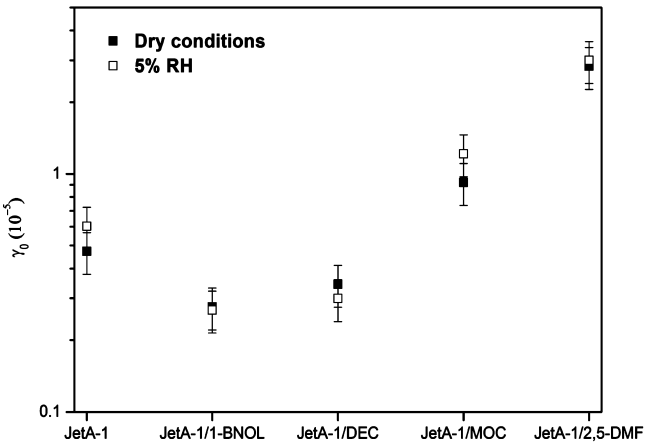

Figure 4. Dependence of γ_0 on type of soot. Experiments were conducted at T = 293 K under dry (0.0032% RH) and 5% RH conditions, solid and open symbols, respectively, using 66 ppbv of NO_2. The BET surface areas measured were used for γ_0 calculations.

to strongly depend on the type of soot. In particular, γ_0 of NO_2 measured on JetA-1/1-BNOL and JetA-1/DEC biosoot surfaces was approximately 2, 3, and 10 times lower than for soot from JetA-1, JetA-1/MOC, and JetA-1/2,5-DMF, respectively. The former observation could possibly be attributed to the different chemical composition of each freshly emitted soot sample.

Figure 5 summarizes the steady-state uptake coefficient of NO_2, γ_{ss}, for all the soot samples analyzed. Under dry conditions, similar values of γ_{ss} were obtained for JetA-1, JetA-1/MOC, and JetA-1/2,5-DMF, while for JetA-1/1-BNOL and JetA-1/DEC biosoots, γ_{ss} was lower by a factor of 2. The addition of H_2O into the reaction system (RH = 5.5%) influenced solely the γ_{ss} of JetA-1 (decreased) and JetA-1/2,5-DMF (increased), whereas no significant changes were observed for the other soot samples. The UV light irradiation of the BC/BrC (J_{NO_2} = 0.012 s^{-1}) had no impact on the γ_{ss}, in the range of the experimental uncertainty of the measurements.

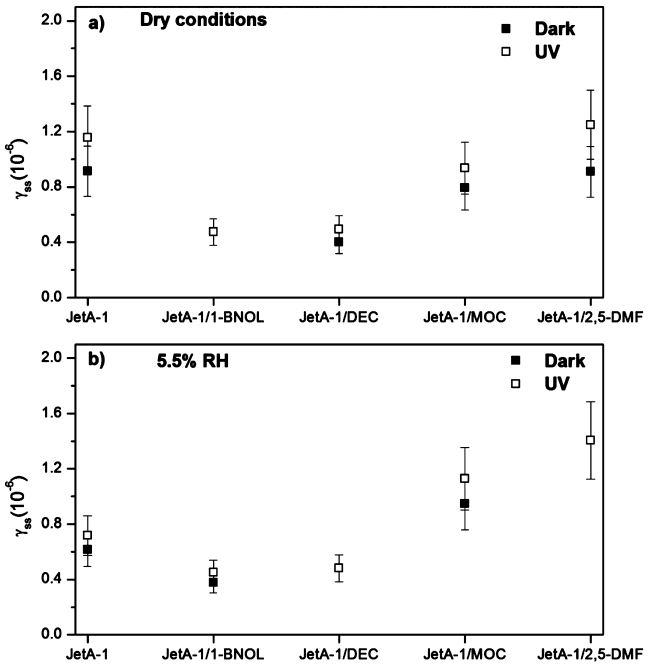

Figure 5. γ_{ss} of NO_2 as a function of soot type under (a) dry conditions (0.0032% RH) and (b) 5% of RH. Experiments were performed at T = 293 K and 66 ppbv of NO_2. Solid and open symbols denote results under dark and UV light irradiation conditions (J_{NO_2} = 0.012 s^{-1}), respectively. Note that for JetA-1/1-BNOL sample under dry conditions, JetA-1/DEC and JetA-1/2,5-DMF under 5.5% of RH there is overlapping of the data points in the graph. The BET surface areas measured were used for γ_{ss} calculations.

The observed data clearly show the following trend regarding the reactive uptake coefficient of NO_2 on the examined soot samples: JetA-1/2,5-DMF > JetA-1/MOC > JetA-1 > JetA-1/DEC ≈ JetA-1/1-BNOL.

A closer analysis of the results obtained for γ_0 and those of γ_{ss} reveals that the observable differences between the soot samples have been attenuated upon NO_2 processing of the soot surfaces. In particular, the initial uptake of NO_2 on JetA-1/2,5-DMF particles was by a factor of 10 higher than that on JetA-1/1-BNOL biosoot, while for the steady-state uptake a factor of 4.6 was obtained; similar attenuation was recorded for the other samples. The former results indicate that processing of the BC/BrC particles with NO_2 lead to depletion of the most active surface sites existing on the freshly emitted soot samples.

Concerning the surface coverage of soot, N_s, it was found to be ~10^{13} molecules cm^{-2}, in agreement with the literature,[11,12] independent of RH and irradiation conditions (Figure 6 and Table 1). JetA-1/1-BNOL and JetA-1/DEC biosoot surfaces displayed similar coverages, $(2-3) \times 10^{13}$ molecules cm^{-2}, while the maximum N_s value was recorded on JetA-1/2,5-DMF surfaces, $N_s \sim 8 \times 10^{13}$ molecules cm^{-2}. However, it should be noted that N_s values should be considered as lower limits because saturation of the surface (which would indicate the end of the reaction) was not achieved within the time scale of the experiment.

3.2.3. Product Yield Determination. In addition to the kinetic measurements presented above, the yield of reaction products formed were determined according to the following expression: $\Delta[\mathrm{product}]/\Delta[NO_2]$. NO and HONO were the only gas-phase products detected, and their distribution is summarized in Figure 7. The formation of nitro-containing

DOI: 10.1021/jp511468t
J. Phys. Chem. A XXXX, XXX, XXX−XXX

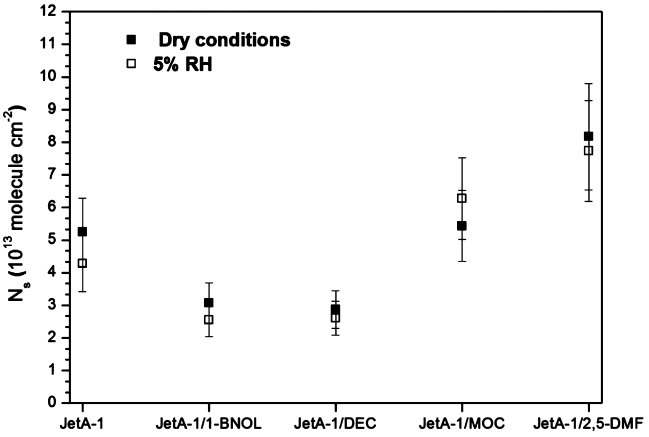

Figure 6. Surface coverage of different types of soot upon their exposition to 66 ppbv of NO_2 at 293 K for 45 min. Solid and open symbols correspond to experiments under dry and humid conditions, 0.0032% and 5% RH, respectively. The BET surface areas measured were used for N_s calculations.

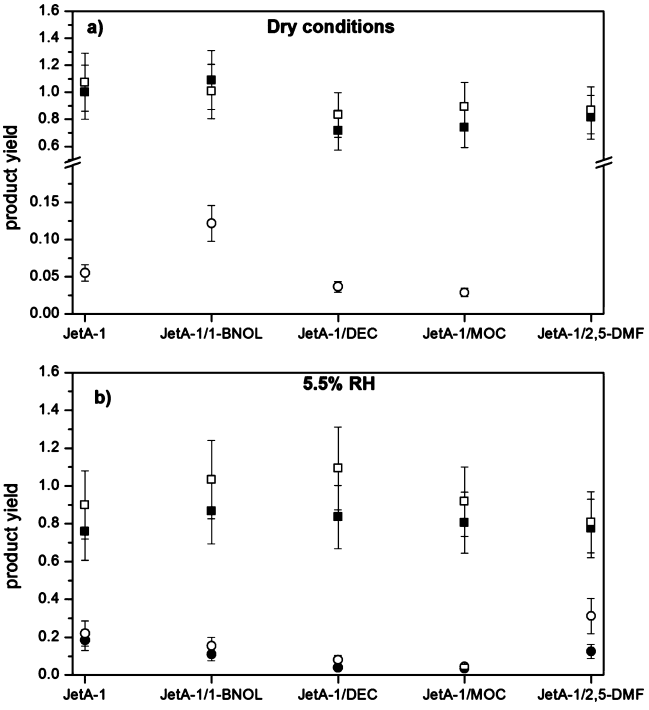

Figure 7. Product yield for NO (squares) and HONO (circles) under dark (solid symbols) and UV irradiation conditions (open symbols) upon exposition of soot surfaces to 66 ppbv of NO_2 at 293 K under (a) dry conditions and (b) 5% RH.

surface products, (Nitro-PAHs, R-NO, R-NO_2, $RONO_2$, etc., R = alkyl group), should not be excluded, although their yield seems to be low, at least under the conditions of the present study. One should note that in our latest study,[14] the formation of several nitroPAH compounds was verified upon processing of kerosene BC/BrC particles with NO_2.

Under dry conditions, NO yields ranged from 80 to 100% while HONO production was limited to <5% for all soot surfaces, except JetA-1/1-BNOL biosoot where it reached 10% and JetA-1/2,5-DMF where HONO was not produced. Similar results were obtained under humid conditions in which NO was the major reaction product. However, HONO production was more pronounced in the presence of H_2O. Indeed, under dark conditions, HONO yield increases up to 20% for pure kerosene and JetA-1/2,5-DMF soot surfaces, while it slightly increased for JetA-1/1-BNOL, >10%; ~5% for JetA-1/MOC; and ~10% for JetA-1/DEC soot. This tendency could be expected because heterogeneous production of HONO is favored on any humid surface that interacts with NO_2.[35,36] Conversely, NO production rates were slightly lower under humid conditions. Note that similar behavior was observed in previous studies from our group in which the interaction of NO_2 with mineral oxide aerosols was studied.[37,38] Finally, the UV irradiation of soot surfaces caused a systematic increase of NO yields, probably because of photodegradation of surface nitro-containing products leading to NO production.

3.3. Solid-Phase Analysis of Soot. One of the major tasks of the current study was the solid-phase analysis of the soot surfaces. The objective was to correlate the chemical reactivity of soot toward NO_2 observed for each fuel, with the chemical composition and the existing functional groups on soot. To this end the analysis of solid soot surfaces was realized with (i) Raman spectroscopy, (ii) NMR, and (iii) HPLC for the determination of PAH compounds on soot.

3.3.1. Raman Spectra. The Raman spectra acquired for conventional and biokerosene soot samples are presented in Figure 8. For sake of clarity, obtained spectra are presented only in the wavelength range of interest, 900−1800 cm^{-1}, where two broad bands appear, with peaks centered at 1330 and 1585 cm^{-1}, corresponding to defective (D) and graphitic (G) bands, respectively. To extract valuable information about the structure and the chemical composition of the soot films, the Raman spectra were deconvoluted. Different fitting methods have been proposed, using Gaussian, Lorentzian, or combination of those functions for peak fitting.[39−42] In addition, the number of the fitting components used is also critical. When using too many components for the same Raman peak, the residual might represent the original spectrum well but most of the produced peaks are without any physical meaning. In the literature, up to 10 fitting peaks have been used to deconvolute Raman spectrum of carbon materials.[40,43,44]

The ratio of the intensities of the D and G bands, I_D/I_G, has been used as an indicative parameter of the degree of disordering of the carbon material.[45] High values of I_D/I_G indicate low graphitic-like structure of the material.[45] The best deconvoluted fit was achieved using a Lorentzian function with two components (for clarity, not shown in Figure 8). The JetA-1/MOC soot sample was the only exception where a "D-side" band, S_D, was observed at ~1200 cm^{-1}; thus a 3 component Lorentzian function was employed to achieve the best fit. G band can stem from two different origins:[41,46] the carbon stretch vibrations of benzene and in general condensed aromatic rings at ~1588 cm^{-1} and C=C sp^2 stretching vibrations of olefinic or conjugated carbon chains.[46] Regarding the origin of the D band, the presence of heavy aromatic compounds with large aromatic rings existing in soot (≥6) is considered to be the major source.[40,47,48] In addition, the wide range of the D bands observed in all soot samples is due to a wide range of aromatic ring size.[40] Therefore, an increased I_D/I_G ratio can be attributed to the formation of aromatic compounds having 6 or more fused benzene rings and provides information about the aromatic/olefinic ratio of the soot sample (the higher the I_D/I_G, the higher the aromatic/olefinic ratio). The presence of the S_D peak after Raman deconvolution of JetA-1/MOC sample is attributed to sp^2 and sp^3 structures.

DOI: 10.1021/jp511468t
J. Phys. Chem. A XXXX, XXX, XXX−XXX

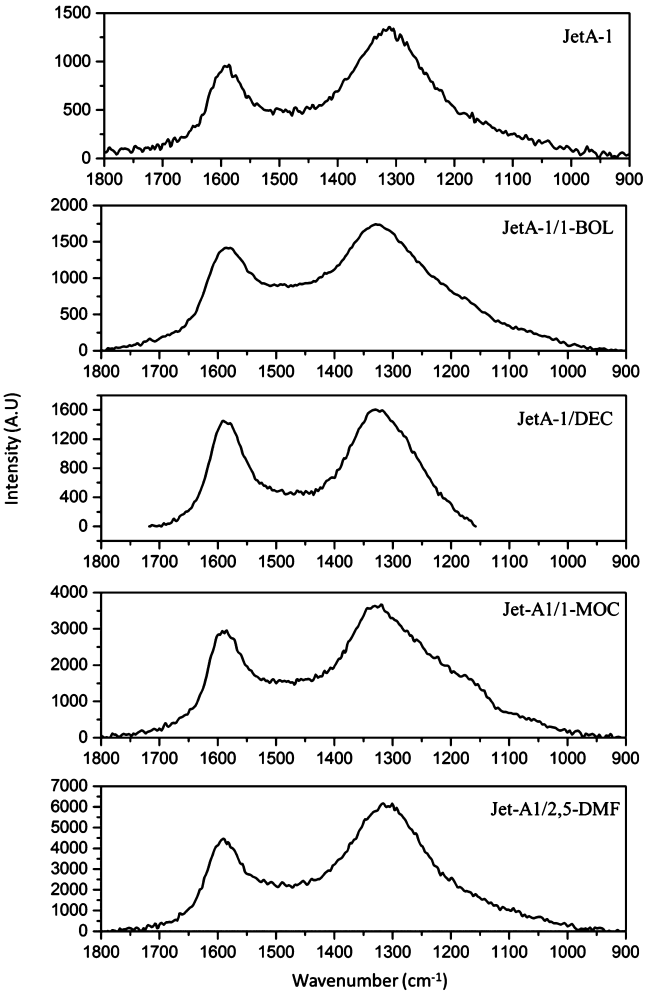

Figure 8. Raman spectra of soot and biosoot samples studied (λ = 780 nm; focused area, 10 μm^2; resolution, R = 2 cm^{-1}). The spectra were focused for presentation purposes.

Compounds such as aryl-alkyl ethers and methyl carbon dangling to aromatic rings contribute to these wavenumbers and are considered to be the major source of this band.[40,41,48]

The values of the I_D/I_G ratios obtained for reference JetA-1 and bio soot samples are presented in Table 1. JetA-1/2,5-DMF appears with the maximum I_D/I_G value followed by pure kerosene, JetA-1/MOC, JetA-1/1-BNOL, and JetA-1/DEC soot surfaces (1.45, 1.41, 1.28, 1.23, and 1.11, respectively). One can note that samples with high chemical reactivity appear with the maximum values of I_D/I_G ratio. This is an indication that the heavy aromatic fraction of soot can possibly influence BC/BrC particle reactivity. However, it should be mentioned that the absolute concentrations of both the aromatic and the aliphatic fractions should be determined.

3.3.2. NMR Analysis. The ^{1}H NMR spectra of the chloroform soluble fraction of the soot samples and the type of chemical groups associated with each signal are presented in Figure S3 of the Supporting Information. One can note that the soot spectra have similar features, which can be explained by the presence of kerosene as the major (80% vol) component in all fuels. Table 2 summarizes the soot characterization data obtained by ^{1}H NMR and reports the proton density of several types of structural units of soot, the CH_2/CH_3 ratio, and the aromatic/aliphatic ratio for the apolar fraction of pure and biosoot samples.

The region δ = 0.5−2.0 corresponds to aliphatic methyl ($-CH_3$) and methylene ($-CH_2-$) soot protons, and the presence of large signals in this region indicates the high amount of alkanes in pure and biosoot samples. The relative ratio of CH_2/CH_3 groups can be used to assess the amount of carbon branching in the soot samples. Except from the JetA-1/MOC soot (2.6), the other soot samples were found to have very similar branching ratios (3.3 ± 0.1), indistinguishable from the value of the pure kerosene soot (3.4). This indicates that branching is not substantially affected by the additive compound used to prepare the bio soot. The high values of branching ratio suggest the existence of alkanes with large and straight chains.

The signals in the region between δ 2.0−2.8 of the NMR spectra represent the presence of methyl and ethyl-substituted aromatic compounds. As can been seen in Table 2, these compounds are present in higher amounts in the JetA-1/1-BNOL and the JetA-1/2,5-DMF, compared to JetA-1, while smaller amounts are observed for the JetA-1/MOC and JetA-1/DEC soot samples. Figure S3 of the Supporting Information shows that the combustion of all fuels leads to the production of R-CH (R is nitrogen or an oxygen atom) protons in the region δ 2.8−4.6 in which the nitrogen atom is chemically connected to aromatic rings. According to Table 2, the JetA-1/1-BNOL soot contains the largest amount of these compounds, followed by the JetA-1/2,5-DMF and JetA-1/DEC soots that contain amounts similar to that of JetA-1 and the JetA-1/MOC soot, which appears to contain the smallest amount of N−CH compounds. In the region δ 4.6−6.2, all the spectra exhibit peaks indicating the presence of very small amounts of vinyl C═CH protons. The low signal in this region indicates the small amount of olefins present in the apolar extracts of all samples.

Table 2. ^{1}H Chemical Shifts in NMR Spectra, the Relative Number of Protons, the Branching Ratio, and the Aromatic/Aliphatic Ratio in Soot Samples

δ (ppm)	hydrogen groups	integration % JetA-1	integration % JetA-1/1-BNOL	integration % JetA-1/DEC	integration % JetA-1/MOC	integration % JetA-1/2,5-DMF
9.5−10.8	O═CH	0.8	0.9	0.6	0.6	0.6
6.5−9.4	Ar	66.0	68.0	61.2	69.0	55.0
4.6−6.2	═CH	0.7	1.0	1.0	0.5	1.0
2.8−4.6	O−CH/N−CH	2.6	3.2	2.6	1.3	2.4
2.0−2.8	Ar−CH	4.0	6.6	4.0	3.3	6.0
1.0−1.4	CH_2	18.0	14.0	21.2	16.0	24.0
0.5−1.0	CH_3	7.9	6.3	9.4	9.3	11.0
CH_2/CH_3 (branching ratio)		3.46	3.33	3.42	2.6	3.24

DOI: 10.1021/jp511468t
J. Phys. Chem. A XXXX, XXX, XXX−XXX

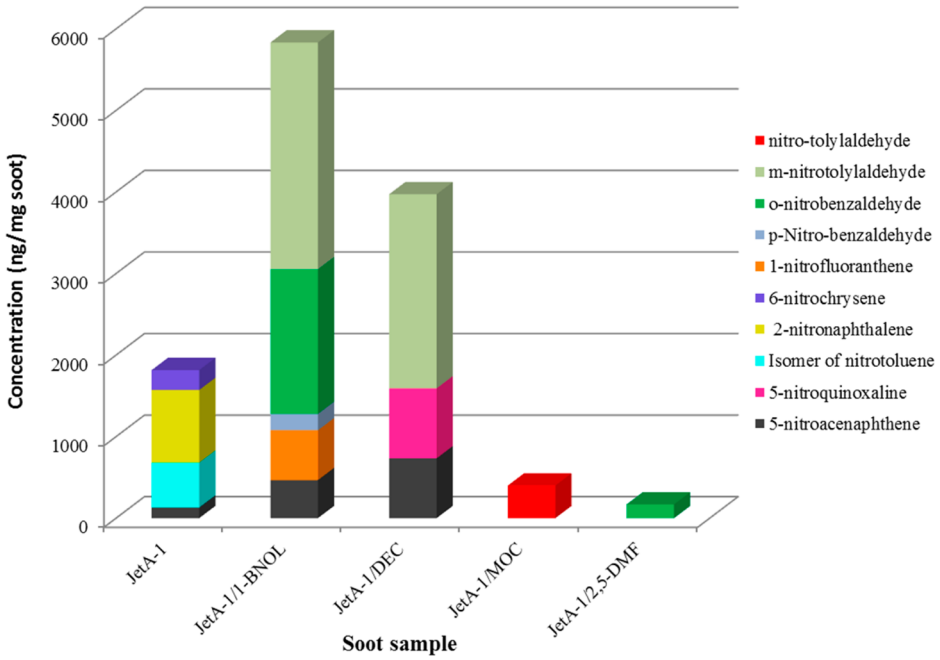

Figure 9. Concentrations of nitro-PAHs detected in soot samples prior to their exposure to NO_2.

A major feature of the spectra of all soot samples is the large amount of signal in the aromatic region δ 6.5−9.4, indicating that the majority of protons in soot have a large aromatic character, with 55−69% of the total protons appearing in this region. It should also be noted that the presence of peaks with chemical shift $9.5 < \delta < 8.0$ in the NMR spectra of the soot samples indicates that a significant amount of PAHs is present in the soot samples. Finally the peaks with chemical shifts δ 9.5−10.8 indicate that the combustion of all fuels leads to the production of aldehydes.

3.3.3. HPLC Analysis. The fresh collected soot samples were analyzed with a HPLC chromatograph coupled with a UV−visible photodiode array detector prior to their exposure to NO_2. The objective of this series of experiments was to analyze the PAH content of the soot samples and find relations between measured concentration of classes of compounds and the observed reactivity of the samples toward NO_2. Seven different classes of PAHs were separated, and more than 200 compounds were identified. The presentation of a detailed list of PAH compounds identified is a subject of ongoing publications from our lab and was beyond the scope of the present study. We present only the results that are correlated with the observed chemical reactivity of soot with NO_2. The HPLC analysis showed that the relative abundance of nitro-PAHs pre-existing on soot (prior to its exposure to NO_2) is the key factor influencing the chemical reactivity. In particular, in Figure 9 the concentrations of the 10 nitro-PAH compounds identified are displayed. JetA-1/1-BNOL (~5800 ng/mg soot) and JetA-1/DEC (~4000 ng/mg soot) were the soot samples with the highest nitro-PAH concentrations, followed by JetA-1 (~1800 ng/mg soot). Regarding the JetA-1/MOC and JetA-1/2,5-DMF samples, their nitro-PAH contents are significantly lower, 400 and 169 ng per mg of soot, respectively. The former observation clearly demonstrates that soot samples containing high concentrations of nitro-PAHs prior to their reaction with NO_2 have lower reactivity toward NO_2. Although this trend appears to be "quite logical", it has never been reported in the past and could be a quite useful prediction factor for soot reactivity with NO_x.

4. SUMMARY AND CONCLUSIONS

The chemical reactivity of soot and biosoot particles toward NO_2 has been studied, and the chemical composition of the soot samples produced were analyzed using Raman spectroscopy, NMR, and HPLC. Furthermore, the BET surface areas were measured and the pore size distributions of the freshly produced BC/BrC particles have been determined by employing NLDFT. To the best of our knowledge, this is the first experimental study in which the reactivity, under relevant atmospheric conditions, and the physicochemical properties of soot particles have been investigated together.

The results showed that the additive compounds used to dope the kerosene fuel influenced the physicochemical properties and reactivity of the corresponding biosoot samples produced. In particular, BET surface measurements and particle size distribution showed that the combustion of JetA-1/2,5-DMF and JetA-1/DEC biofuels produced soot particles with the highest and lowest surface area and pore volume, respectively (Figure 2, Figure S1 of the Supporting Information, and Table 1). Conversely, no significant differences have been observed between the other Br/BrC particles.

The degradation of NO_2 over the soot particles was found to depend on the substrate BC/BrC sample. Using JetA-1 as the reference fuel, JetA-1/2,5-DMF and JetA-1/MOC appeared to be more reactive, while for JetA-1/1-BNOL and JetA-1/DEC NO_2 reactivity was significantly decreased. These differences were observed at the maximum extent within the first minutes of the NO_2−soot interaction, where γ_0 was measured, and were attenuated upon processing of soot particles for longer time, γ_{ss}. This attenuation was attributed to the depletion of the most reactive surface sites of soot within the first minutes of the interaction. UV illumination of the surface did not accelerate the uptake process, at least to an extent that could be clearly measured and not be attributed to experimental uncertainties. Regarding the products, NO was measured to be the major

DOI: 10.1021/jp511468t
J. Phys. Chem. A XXXX, XXX, XXX−XXX

product, ranging from 80% to 100%, while HONO production was limited to significantly lower limits (<20%). Irradiating the soot surfaces with UV light caused a slight but systematic increase of NO production, probably due to the degradation of surface products formed.

When attempts were made to correlate the chemical reactivity with the physicochemical properties of soot particles, the following interesting conclusions were drawn:

1. The combustion of fuels with high soot collection rate appeared to have also high chemical reactivity toward NO_2. Several studies in the literature have reported a similar effect; nevertheless, a substantive response has never been addressed on this issue, which was simply attributed to differences in combustion conditions.[49] A possible explanation could be that soot oxidation state follows an inverse dependence with collection rate of soot (lower sooting, higher oxidation state of soot). Previous studies in our lab and in the literature have shown that soot oxidation decreases significantly its chemical reactivity.[13]

2. Soot samples with high BET surface area and pore size distributions were more reactive toward NO_2. This indicates that the physical properties of the particles can affect the reactivity of a surface.

3. The Raman analysis results showed that the ratio of the heavy aromatic/olefinic fraction contained in soot is an indicator for surface reactivity. The higher the heavy aromatic/olefinic ratio, the higher the reactivity. However, to assess the impact of aromatic fraction on the chemical reactivity, the absolute concentrations (or at least the relative abundance) in each of the soot samples should be determined and compared. This is the goal of ongoing studies from our group. Indeed, the soot samples containing high quantities of aromatics, i.e., JetA-1/2,5-DMF and JetA-1/MOC biosoots, appeared to have the highest reactivity in our study. Finally, it should be noted that the analysis of the aliphatic fraction was beyond the scope of our studies. Nevertheless, it could also affect the chemical reactivity.

4. The HPLC analysis showed that soot samples containing higher quantities of nitro-PAHs or nitro-containing species had the lowest reactivity toward NO_2. It is possible that the surface sites that would be available to react with NO_2 upon processing of the soot particles in our experiments have already reacted during the combustion process with the NO_x formed. Although this conclusion seems to be reasonable, it has never been reported in the past and could be a quite useful prediction factor for soot reactivity with NO_x. The higher the concentrations of nitro-containing species in soot samples formed during the combustion, the lower their reactivity toward NO_x.

To conclude, our results indicate that the nature of the additive compound in biofuel influences the chemical properties and reactivity toward NO_2. In addition, the oxygen content of the biofuels is not an indicative factor of soot reactivity. Regarding the atmospheric implications, it seems that the utilization of biofuels will not significantly impact the chemical degradation of NO_x on biosoot particles. Nevertheless biofuels might have an important impact on the hygroscopicity of the corresponding biosoot particles. Preliminary results in our lab have shown that the combustion of biofuels containing oxygenated additives produce a significantly higher amount of soot surface-bound polar PAHs compared to conventional fuels. The former observation could be critical for the cloud radiative properties because soot acts as CCN. The high concentration of the polar PAH fraction could also have a significant impact on human health. Upon the removal of soot particles from the atmosphere (mainly due to precipitation), this class of compounds could be dissolved and enter the hydrologic cycle.

■ ASSOCIATED CONTENT

Supporting Information

A table presenting the experimental combustion condition used for each fuel, schematic representation of the two experimental setups used (Figure S1), the soot and biosoot particle size distributions (Figure S2), and the NMR spectra of the JetA-1 and JetA-1/biosoot samples (Figure S3). This material is available free of charge via the Internet at http://pubs.acs.org.

■ AUTHOR INFORMATION

Corresponding Authors

*Tel.: +33 238255492. Fax: +33 238696004. E-mail: manolis.romanias@cnrs-orleans.fr.

*Tel.: +33 238255466. Fax: +33 238696004. E-mail: philippe.dagaut@cnrs-orleans.fr.

Notes

The authors declare no competing financial interest.

■ ACKNOWLEDGMENTS

The research leading to these results has received funding from the European Research Council under the European Community's Seventh Framework Programme (FP7/2007-2013)/ERC Grant Agreement 291049-2G-CSafe.

■ REFERENCES

(1) United Nations Population Information Network. http://www.un.org/popin/, in 2013.

(2) Agarwal, A. K. Biofuels (Alcohols and Biodiesel) Applications as Fuels for Internal Combustion Engines. *Prog. Energy Combust. Sci.* **2007**, *33*, 233−271.

(3) Hajbabaei, M.; Johnson, K. C.; Okamoto, R. A.; Mitchell, A.; Pullman, M.; Durbin, T. D. Evaluation of the Impacts of Biodiesel and Second Generation Biofuels on NOx Emissions for CARB Diesel Fuels. *Environ. Sci. Technol.* **2012**, *46*, 9163−9173.

(4) Robbins, C.; Hoekman, S.; Ceniceros, E.; Natarajan, M. Effects of Biodiesel Fuels Upon Criteria Emissions.*SAE Technical Paper 2011-01-1943*, 2011, DOI: 10.4271/2011-01-1943

(5) Poschl, U. Atmospheric Aerosols: Composition, Transformation, Climate and Health Effects. *Angew. Chem., Int. Ed.* **2005**, *44*, 7520−7540.

(6) Daly, H. M.; Horn, A. B. Heterogeneous Chemistry of Toluene, Kerosene and Diesel Soots. *Phys. Chem. Chem. Phys.* **2009**, *11*, 1069−1076.

(7) Kirchner, U.; Scheer, V.; Vogt, R. FTIR Spectroscopic Investigation of the Mechanism and Kinetics of the Heterogeneous Reactions of NO_2 and HNO_3 with Soot. *J. Phys. Chem. A* **2000**, *104*, 8908−8915.

(8) Bond, T. C.; Doherty, S. J.; Fahey, D. W.; Forster, P. M.; Berntsen, T.; DeAngelo, B. J.; Flanner, M. G.; Ghan, S.; Kärcher, B.; Koch, D.; et al. Bounding the Role of Black Carbon in the Climate System: A Scientific Assessment. *J. Geophys. Res. [Atmos.]* **2013**, *118*, 5380−5552.

(9) Cooke, W. F.; Wilson, J. J. N. A Global Black Carbon Aerosol Model. *J. Geophys. Res. [Atmos.]* **1996**, *101*, 19395−19409.

(10) Hauglustaine, D. A.; Ridley, B. A.; Solomon, S.; Hess, P. G.; Madronich, S. HNO_3/NO_x Ratio in the Remote Troposphere During MLOPEX 2: Evidence for Nitric Acid Reduction on Carbonaceous Aerosols? *J. Geophys. Res. [Atmos.]* **1996**, *23*, 2609−2612.

DOI: 10.1021/jp511468t
J. Phys. Chem. A XXXX, XXX, XXX−XXX

(11) Lelievre, S.; Bedjanian, Y.; Laverdet, G.; Le Bras, G. Heterogeneous Reaction of NO_2 with Hydrocarbon Flame Soot. *J. Phys. Chem. A* **2004**, *108*, 10807−10817.
(12) Aubin, D. G.; Abbatt, J. P. D. Interaction of NO_2 with Hydrocarbon Soot: Focus on HONO Yield, Surface Modification, and Mechanism. *J. Phys. Chem. A* **2007**, *111*, 6263−6273.
(13) Lelievre, S.; Bedjanian, Y.; Pouvesle, N.; Delfau, J.-L.; Vovelle, C.; Le Bras, G. Heterogeneous Reaction of Ozone with Hydrocarbon Flame Soot. *Phys. Chem. Chem. Phys.* **2004**, *6*, 1181−1191.
(14) Romanias, M. N.; Bedjanian, Y.; Zaras, A. M.; Andrade-Eiroa, A.; Shahla, R.; Dagaut, P.; Philippidis, A. Mineral Oxides Change the Atmospheric Reactivity of Soot: NO_2 Uptake under Dark and UV Irradiation Conditions. *J. Phys. Chem. A* **2013**, *117*, 12897−12911.
(15) Bedjanian, Y.; Nguyen, M. L. Kinetics of the Reactions of Soot Surface-Bound Polycyclic Aromatic Hydrocarbons with O_3. *Chemosphere* **2010**, *79*, 387−393.
(16) Guilloteau, A. l.; Nguyen, M. L.; Bedjanian, Y.; Le Bras, G. Desorption of Polycyclic Aromatic Hydrocarbons from Soot Surface: Pyrene and Fluoranthene. *J. Phys. Chem. A* **2008**, *112*, 10552−10559.
(17) Kee, R. J.; Rupley, F. M.; Miller, J. A. *CHEMKIN-II: A Fortran Chemical Kinetics Package for the Analysis of Gas-Phase Chemical Kinetics*; SAND89−8009; Sandia National Laboratories: Albuquerque, NM, 1989.
(18) Brunauer, S. Pore Structure of Solids. *Pure Appl. Chem.* **1976**, *48*, 401−405.
(19) Dombrowski, R. J.; Hyduke, D. R.; Lastoskie, C. M. Pore Size Analysis of Activated Carbons from Argon and Nitrogen Porosimetry Using Density Functional Theory. *Langmuir* **2000**, *16*, 5041−5050.
(20) Fashandi, H.; Karimi, M. Characterization of Porosity of Polystyrene Fibers Electrospun at Humid Atmosphere. *Thermochim. Acta* **2012**, *547*, 38−46.
(21) Kowalczyk, P.; Terzyk, A. P.; Gauden, P. A.; Leboda, R.; Szmechtig-Gauden, E.; Rychlicki, G.; Ryu, Z. Y.; Rong, H. Q. Estimation of the Pore-size Distribution Function from the Nitrogen Adsorption Isotherm. Comparison of Density Functional Theory and the Method of Do and Co-workers. *Carbon* **2003**, *41*, 1113−1125.
(22) Landers, J.; Gor, G. Y.; Neimark, A. V. Density Functional Theory Methods for Characterization of Porous Materials. *Colloids Surf., A* **2013**, *437*, 3−43.
(23) Neimark, A. V.; Ravikovitch, P. I.; Grün, M.; Schüth, F.; Unger, K. K. Pore Size Analysis of MCM-41 Type Adsorbents by Means of Nitrogen and Argon Adsorption. *J. Colloid Interface Sci.* **1998**, *207*, 159−169.
(24) Ravikovitch, P. I.; Neimark, A. V. Characterization of Micro- and Mesoporosity in SBA-15 Materials from Adsorption Data by the NLDFT Method. *J. Phys. Chem. B* **2001**, *105*, 6817−6823.
(25) Romanias, M. N.; El Zein, A.; Bedjanian, Y. Heterogeneous Interaction of H_2O_2 with TiO_2 Surface under Dark and UV Light Irradiation Conditions. *J. Phys. Chem. A* **2012**, *116*, 8191−8200.
(26) Bedjanian, Y.; Romanias, M. N.; El Zein, A. Interaction of OH Radicals with Arizona Test Dust: Uptake and products. *J. Phys. Chem. A* **2013**, *117*, 393−400.
(27) Romanias, M. N.; El Zein, A.; Bedjanian, Y. Reactive Uptake of HONO on Aluminium Oxide Surface. *J. Photochem. Photobiol., A* **2012**, *250*, 50−57.
(28) Romanias, M. N.; El Zein, A.; Bedjanian, Y. Uptake of Hydrogen Peroxide on the Surface of Al_2O_3 and Fe_2O_3. *Atmos. Environ.* **2013**, *77*, 1−8.
(29) El Zein, A.; Bedjanian, Y. Interaction of NO_2 with TiO_2 Surface under UV Irradiation: Measurements of the Uptake Coefficient. *Atmos. Chem. Phys.* **2012**, *12*, 1013−1020.
(30) Barnard, J. C.; Chapman, E. G.; Fast, J. D.; Schmelzer, J. R.; Slusser, J. R.; Shetter, R. E. An Evaluation of the FAST-J Photolysis Algorithm for Predicting Nitrogen Dioxide Photolysis Rates under Clear and Cloudy Sky Conditions. *Atmos. Environ.* **2004**, *38*, 3393−3403.
(31) Castro, T.; Rouiz-Squarez, G. L.; Gay, C. Direct Measurement of NO_2 Photolysis Rates for Mexico City. *Atmosfera* **1995**, *8*, 137−142.
(32) Kraus, A.; Hofzumahaus, A. Field Measurements of Atmospheric Photolysis Frequencies for O_3, NO_2, HCHO, CH_3CHO, H_2O_2, and HONO by UV Spectroradiometry. *J. Atmos. Chem.* **1998**, *31*, 161−180.
(33) Frank-Kamenetskii, D. A. *Diffusion and Heat Transfer in Chemical Kinetics*; Plenum Press: New York, 1969.
(34) Andrade-Eiroa, A.; Shahla, R.; Romanias, M. N.; Dagaut, P. An Alternative to Trial and Error Methodology in Solid Phase Extraction: An Original Automated Solid Phase Extraction Procedure for Analysing PAHs and PAH-Derivatives in Soot. *RSC Adv.* **2014**, *4*, 42271−42271.
(35) Longfellow, C. A.; Ravishankara, A. R.; Hanson, D. R. Reactive Uptake on Hydrocarbon Soot: Focus on NO_2. *J. Geophys. Res. [Atmos.]* **1999**, *104*, 13833−13840.
(36) Kleffmann, J.; H. Becker, K.; Lackhoff, M.; Wiesen, P. Heterogeneous Conversion of NO_2 on Carbonaceous Surfaces. *Phys. Chem. Chem. Phys.* **1999**, *1*, 5443−5450.
(37) McEnally, C. S.; Pfefferle, L. D. Sooting Tendencies of Oxygenated Hydrocarbons in Laboratory-Scale Flames. *Environ. Sci. Technol.* **2011**, *45*, 2498−2503.
(38) McMurry, P. H.; Litchy, M.; Huang, P.-F.; Cai, X.; Turpin, B. J.; Dick, W. D.; Hanson, A. Elemental Composition and Morphology of Individual Particles Separated by Size and Hygroscopicity with the TDMA. *Atmos. Environ.* **1996**, *30*, 101−108.
(39) Knauer, M.; Schuster, M. E.; Su, D.; Schlögl, R.; Niessner, R.; Ivleva, N. P. Soot Structure and Reactivity Analysis by Raman Microspectroscopy, Temperature-Programmed Oxidation, and High-Resolution Transmission Electron Microscopy. *J. Phys. Chem. A* **2009**, *113*, 13871−13880.
(40) Li, X. J.; Hayashi, J.; Li, C. Z. FT-Raman Spectroscopic Study of the Evolution of Char Structure During the Pyrolysis of a Victorian Brown Coal. *Fuel* **2006**, *85*, 1700−1707.
(41) Schwan, J.; Ulrich, S.; Batori, V.; Ehrhardt, H.; Silva, S. R. P. Raman Spectroscopy on Amorphous Carbon Films. *J. Appl. Phys.* **1996**, *80*, 440−447.
(42) Chu, P. K.; Li, L. H. Characterization of Amorphous and Nanocrystalline Carbon Films. *Mater. Chem. Phys.* **2006**, *96*, 253−277.
(43) Nathan, M. I.; Smith, J. E.; Tu, K. N. Raman-Spectra of Glassy Carbon. *J. Appl. Phys.* **1974**, *45*, 2370−2370.
(44) Robertson, J. Properties of Diamond-like Carbon. *Surf. Coat. Technol.* **1992**, *50*, 185−203.
(45) Tuinstra, F.; Koenig, J. L. Raman Spectrum of Graphite. *J. Chem. Phys.* **1970**, *53*, 1126−1130.
(46) Tamor, M. A.; Vassell, W. C. Raman "Fingerprinting" of Amorphous Carbon Films. *J. Appl. Phys.* **1994**, *76*, 3823−3830.
(47) Wang, Y.; Alsmeyer, D. C.; McCreery, R. L. Raman-Spectroscopy of Carbon Materials - Structural Basis of Observed Spectra. *Chem. Mater.* **1990**, *2*, 557−563.
(48) Lin-Vien, D.; Colthup, B. N.; Fateley, G. W.; Grasselli, G. J. Appendix 3 - A Summary of Characteristic Raman and Infrared Frequencies. In *The Handbook of Infrared and Raman Characteristic Frequencies of Organic Molecules*; Academic Press: San Diego, CA, 1991; pp 477−490.
(49) Alcala-Jornod, C.; van den Bergh, H.; Rossi, M. J. Reactivity of NO_2 and H_2O on Soot Generated in the Laboratory: A Diffusion Tube Study at Ambient Temperature. *Phys. Chem. Chem. Phys.* **2000**, *2*, 5584−5593.

DOI: 10.1021/jp511468t
J. Phys. Chem. A XXXX, XXX, XXX−XXX